

Thermionic emission from surface-terminated nanocrystalline diamond

Vance S. Robinson^a, Yoshiyuki Show^b, Greg M. Swain^b,
Ronald G. Reifenberger^a, Timothy S. Fisher^{a,*}

^a Birck Nanotechnology Center, Purdue University, 1205 W. State St., West Lafayette, IN 47907-2057, United States

^b Department of Chemistry Michigan State University East Lansing, MI 48824, United States

Received 1 July 2005; received in revised form 18 January 2006; accepted 22 January 2006

Available online 9 March 2006

Abstract

Thermionic electron emission forms the basis of both electron sources for a variety of applications and a direct energy conversion process that is compact and scalable. The present study characterizes thermionic emission from boron-doped nanocrystalline diamond films with hydrogen and nitrophenyl surface termination layers. A hemispherical energy analyzer was used to measure electron energy distributions from the emitters at elevated temperatures. Thermionic emission energy distributions, acquired at temperatures ranging from 700 to 1100°C, reveal that emission occurs from regions of differing work functions. The relative peak intensities, representing each work function, change with temperature indicating instability in the emitter's surface chemistry. Corresponding partial pressure measurements of pertinent gases present in the chamber during the experiment were collected by a residual gas analyzer and support the hypothesis of unstable surface chemistry. The lowest work functions measured for the hydrogen- and nitrophenyl-terminated films were 3.95 and 3.88 eV, respectively. After the initial heating cycle, the hydrogen-terminated sample's surface was regenerated by exposure to hydrogen plasma. The lower work function was restored by this process, and the resulting thermionic electron energy distributions again were indicative of surface desorption.

© 2006 Elsevier B.V. All rights reserved.

Keywords: Thermionic emission; Nanocrystalline diamond; Electron energy analyzer; Surface termination

1. Introduction

Thermionic emitters are used as electron sources in many contemporary applications such as fluorescent lighting, cathode ray tubes, X-ray tubes, mass spectrometers, vacuum gauges, scanning electron microscopes, and other scientific instruments. Most such sources are resistively heated filaments that produce a flow of electrons. Further, thermionic emission provides a means of converting heat directly into electrical power. Such thermionic converters have been designed to operate in conjunction with various heat sources, such as solar radiation, nuclear reactions, and the combustion of fossil fuels [1–6]. Some of this technology's more attractive qualities include: compactness, scalability, and high waste heat rejection temperatures for cascaded systems [3,7]. Harnessing thermionic power generation for efficient direct energy conversion is the underlying motivation of this work.

In an effort to improve the thermodynamic efficiency and capacity of electron emission, low-work-function materials must be developed [8–10]. The properties of chemical vapor deposited diamond with a hydrogen surface termination have been investigated by several groups, who have demonstrated that hydrogen-terminated boron-doped diamond has a negative electron affinity [11–13], and a hydrogen-terminated nanocrystalline diamond (HND) sample is tested in this work. A nitrophenyl-terminated nanocrystalline diamond (NND) sample is included in this study because nitrophenyl termination represents the successful modification of an otherwise non-reactive surface with significant potential for electrochemical applications [14,15]. Surface temperature can affect the stability of such termination layers, and the present work investigates the stability and performance of hydrogen and nitrophenyl surface terminations on nanocrystalline diamond films at elevated temperatures.

Subsequent sections of this paper describe results from thermionic emission testing of different nanocrystalline diamond films in detail. First, thermionic emission theory and its relation to thermionic electron energy distributions (TEEDs) are

* Corresponding author. Tel.: +1 765 494 5627.

E-mail address: tsfisher@purdue.edu (T.S. Fisher).

described. This section also includes a discussion of instrument effects on the reported measurements. Following the theory section is a description of the experimental setup and the diamond film deposition process. TEED results and corresponding theoretical curves are presented along with applicable partial pressure results in the following section. A brief conclusion follows, summarizing the results and the main contributions of this work.

2. Theory

The thermionic emission energy distribution (TEED) from a free-electron metal is given by [16]:

$$J'(E) = \frac{4\pi m q}{\hbar^3} \frac{(E-\phi)}{1 + \exp\left(\frac{E}{k_B T}\right)}. \quad (1)$$

The terms m , q , and \hbar are the electron mass, electron charge and reduced Planck's constant ($h/2\pi$), respectively. The term E represents electron energy; ϕ is the material's work function; k_B is Boltzman's constant; and T represents the temperature of the emitter surface. The energy distribution is symbolized by J' because it is the energy derivative of the saturation current density, J . Differentiation of Eq. (1) with respect to electron energy E reveals that the maximum thermionic emission intensity occurs at an energy that is $k_B T$ greater than the work function. The foregoing relationship is used in subsequent sections to estimate work functions from the measured energies at maximum intensity. Integration of Eq. (1) over all energies from the ϕ to infinity gives the familiar Richardson–Dushman equation [17]:

$$J = A^* T^2 \exp\left[\frac{-\phi}{k_B T}\right], \quad (2)$$

where A^* represents the apparent emission constant [18].

In this study, a hemispherical energy analyzer was used to measure TEEDs. The actual measured energy distribution is a convolution of the distribution produced by the emitter and a Gaussian instrument spreading function, which is determined by specific analyzer parameters [19,20]. The form of the instrument function is given by

$$G_I = \frac{1}{\sigma\sqrt{2\pi}} \exp\left[-\frac{1}{2}\left(\frac{E-E'}{\sigma}\right)^2\right]. \quad (3)$$

The standard deviation σ is the term through which analyzer parameters affect the function and is subsequently referred to as the 'analyzer resolution'. The convolution of Eqs. (1) and (3) represents the energy distribution reported by the analyzer that is subsequently used to quantify shifts in relative peak intensities:

$$J'_{observed} = \sum_{i=1}^n A_i [G_I^* I_i(\phi_i)]. \quad (4)$$

where A_i is called the area coefficient because its magnitude is proportional to the area of the sample that emits electrons at or

above the effective work function ϕ_i with an intensity I_i . The summation accounts for the possibility of multiple regions on the surface of the emitting material of differing effective work functions ϕ_i .

In the present work, we interpret thermionic energy distributions through an effective mass approximation theory modified by the Gaussian instrument function. The effective mass approximation is expected to be reasonable given that prior work by Köch et al. [11] on thermionic field emission from polycrystalline diamond has revealed relatively uniform surface emission intensities explained by the thermal excitation of electrons into the conduction band of a low-electron-affinity surface. We also note that the effective mass model does not alter the shape of the distribution predicted by free-electron theory, given that the mass term is a pre-factor in the energy distribution [see Eq. (1)] that is normalized in the presented results. These approximations are also consistent, for example, with the use of Fowler–Nordheim theory, which is based on free-electron theory, in interpretation of field emission from polycrystalline diamond [21].

3. Experimental setup

Thermionic energy distributions were measured with a hemispherical energy analyzer (SPECS-Phoibos 100 SCD) connected to a vacuum chamber that achieves pressures of the order of 10^{-8} Torr. The heated emitter sample is located at the focal plane, 40 mm below the analyzer's aperture. The temperature of the molybdenum heater (HeatWave Labs, Inc.) is measured by a K-type thermocouple embedded 1 mm below the top surface and is modulated a PID-controlled power supply. Due to contact resistance and other radiative heat losses between the surface of the sample and the thermocouple, the temperature measurements can exceed the surface temperature of the sample by as much as 30 °C. All energy distributions reported in this study were made after the temperature of the emitter had stabilized for at least 20 min.

The heater assembly is thermally and electrically isolated from the chamber by alumina hardware. The heater is negatively biased (-2 V) to accelerate electrons into the analyzer and to

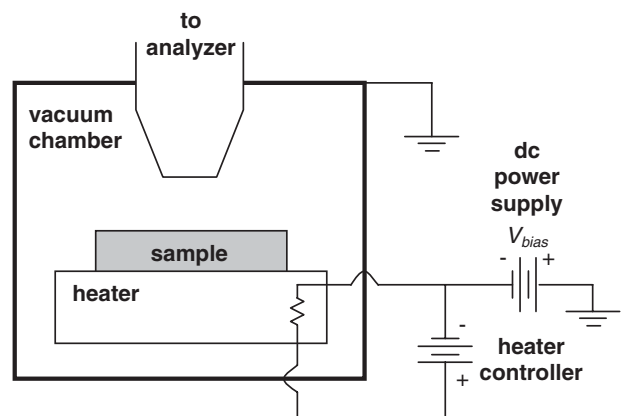


Fig. 1. Schematic of the experimental setup for measuring TEEDs including the four main components: energy analyzer, heater, heater controller, and power supply.

ensure that they have sufficient energy to overcome the work function of the analyzer (4.12 eV). Electron acceleration was achieved by connecting the heater to a DC power supply (Hewlett Packard 6542A) and grounding the analyzer's aperture (see Fig. 1). Voltage sense lines for the DC power supply were implemented, reducing the uncertainty in the acceleration voltage to ± 0.3 mV. A residual gas analyzer (RGA, Inficon Transpector 2) was used to measure changes in partial pressure in the vacuum chamber that could represent changes in the surface chemistry of the sample, and we note that operating the RGA in conjunction with the analyzer caused a moderate increase in instrument broadening.

4. Nanocrystalline diamond film growth

Nanocrystalline boron-doped diamond (BND) thin films were deposited using microwave-assisted plasma enhanced chemical vapor deposition (1.5 kW, 2.54 GHz, Astex, Inc., Lowell, MA) on highly conducting p-Si (100) substrates ($< 0.001 \Omega\text{-cm}$, Virginia Semiconductor, Inc.). The substrates were pretreated by mechanical polishing on a felt pad using a $0.1 \mu\text{m}$ diameter diamond powder slurry in water (GE Superabrasives, Worthington, OH). The scratched substrates were then ultrasonically cleaned in ultrapure water, isopropyl alcohol (IPA), acetone, IPA, and ultrapure water to remove polishing debris from the surface. Embedded diamond particles and polishing striations likely both serve as initial nucleation sites for diamond growth. Increasing the nucleation density and nucleation rate of diamond growth on nondiamond substrates through substrate pretreatment has been the subject of much research over the years, and it is well established that scratching defects and diamond particles function as nucleation sites for CVD diamond growth [22]. The nanocrystalline diamond films were deposited at 800 W, using an Ar/H₂/CH₄/B₂H₆ source gas mixture consisting of 1% CH₄/H₂ + Ar with 10 ppm B₂H₆ added for boron doping. The system pressure was 140 Torr, the substrate temperature was ca. 800 °C (estimated via an optical pyrometer), and the growth time was 2 h. All gases were ultrahigh purity grade (99.999%, AGA Specialty Gas, Cleveland, OH). The resulting film thickness was approximately 2 μm .

Following the deposition, the CH₄ and B₂H₆ flows were stopped, and the films remained exposed to the H₂/Ar plasma for an additional 10 min. The argon flow was then stopped, and the plasma power and pressure were slowly reduced over a 5 min. period to cool the samples in the presence of atomic hydrogen to a temperature below 400 °C. The plasma power was then turned off, and the films cooled to room temperature under a flow of H₂. This post-growth annealing in a hydrogen plasma serves to etch away adventitious non-diamond carbon impurities, to minimize dangling bonds, and to ensure maximum hydrogen termination. The films had a nominal boron dopant concentration of 10^{20}B cm^{-3} and a film resistivity of less than $0.05 \Omega\text{-cm}$. Typical carrier concentrations (holes) are in the low 10^{20}cm^{-3} range, and carrier mobilities are between 0.1 and $1 \text{cm}^2/\text{V-s}$, as determined from Hall Effect measurements.

At this point, the fabrication of the hydrogen-terminated (HND) film is complete. Further processing was required for the

NND film. Boron-doped nanocrystalline diamond was chemically modified with nitrophenyl groups via the electroreduction of 4-nitrophenyl diazonium salt [14,15,23–25]. The $1e^-$ reduction reaction leads to the formation of a nitrophenyl radical at the electrode surface, which then reacts with a surface atom and attaches via a covalent bond. This electrochemically assisted chemical modification scheme is a very versatile method for controlling the surface chemistry of conductors and semiconductors with a wide variety of substituted aryl molecules. We suppose that the covalent attachment of the nitrophenyl group requires the formation of at least two nitrophenyl radicals. One radical generates the “active” site on the hydrogen-terminated diamond surface by abstracting a hydrogen atom. The second nitrophenyl radical then couples at the newly formed radical site on the surface. Fig. 2 contains an SEM image of the HND film in which the sub-micrometer crystal facets are evident.

5. Results

Three TEEDs, corresponding to three temperature conditions, were recorded for each sample: at approximately 750 °C, at a maximum temperature above 1090 °C, and again at 750 °C. During the heating cycle, the residual gas analyzer monitored partial pressures of relevant chemical species inside the chamber that could represent desorption of the termination layer. The following subsections describe the validation of the experiment and thermionic emission results from the various samples.

5.1. Experiment validation

Before measuring thermionic emission from the nanocrystalline diamond films, emission from a material with known work function was measured. The material was single-crystal tungsten (100), selected for its well documented work function in the range of 4.52 to 4.59 eV [26–28]. Fig. 3 shows a thermionic emission energy distribution from tungsten at approximately 900 °C. The sharp increase in intensity followed by a gently sloping high-energy tail is typical of thermionic emission [29].

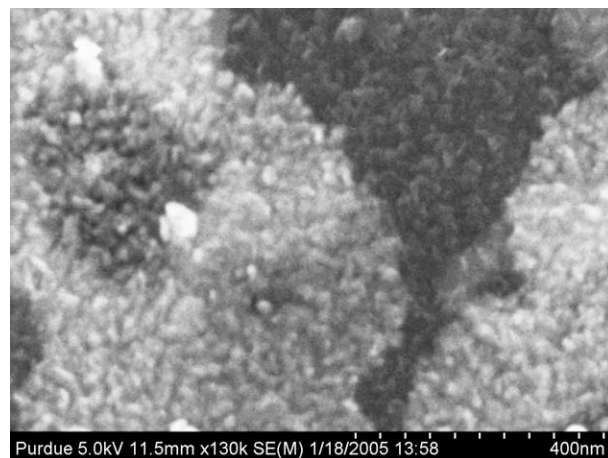


Fig. 2. SEM image of the HND sample. Regions of differing work function are likely for such heterogeneous surface. The length scale confirms nanoscale crystal structure.

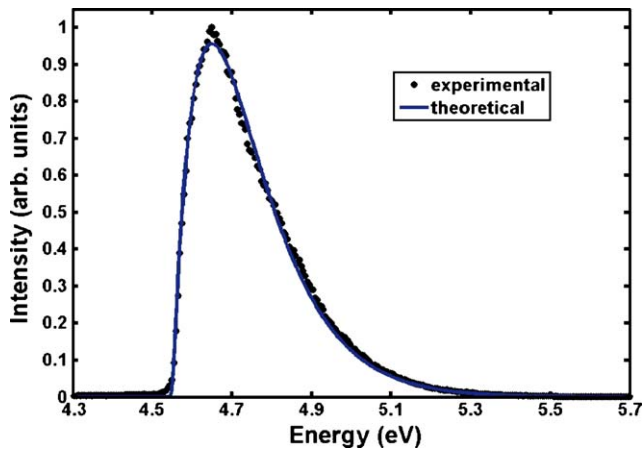


Fig. 3. TEED from single-crystal tungsten at 900°C used to validate the experimental setup.

Based on the curve fit to the data in Fig. 3, the work function of the single-crystal tungsten sample is 4.56 eV, consistent with the literature. These results for thermionic emission from tungsten serve to validate the experimental setup used in this study.

5.2. Hydrogen-terminated nanocrystalline diamond (HND)

TEEDs from the HND substrate deviate from a homogeneous free-electron emitter as shown in Fig. 4, where the distributions contain a secondary increase in intensity. Recalling Eq. (4), additional peaks are interpreted as areas on the surface of the emitter with different effective work functions. In Fig. 4, the high-energy shoulder of the TEED at 750°C before the maximum temperature becomes the dominant peak at the maximum temperature (1085°C). Subsequently, the dominant peak in the TEED before the maximum temperature reduces to the leading shoulder seen in the TEED at 750°C after the maximum temperature. Table 1 summarizes the important features of the three TEEDs for the HND sample, the locations of their respective peaks, and the corresponding work functions.

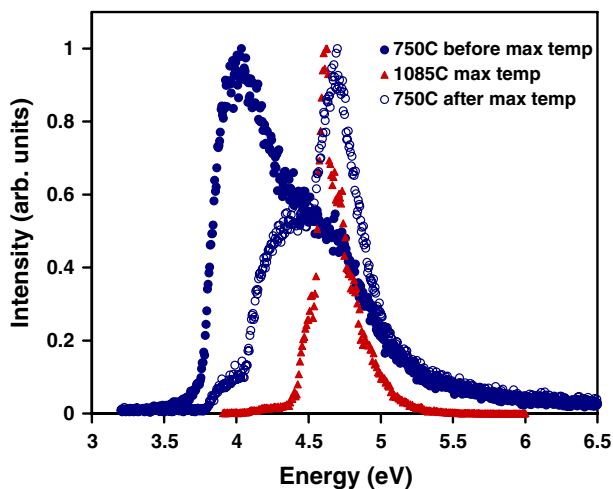


Fig. 4. TEEDs from a hydrogen-terminated nanocrystalline diamond measured at 750, 1085 and 750°C. The shift in the energy at maximum intensity before and after the maximum temperature indicates that the relative area of higher work function has increased in size.

Table 1

Resolution, energy of peak intensity, and effective work function of TEEDs from the HND sample

TEED	Temperature (°C)	Energy at max. intensity (eV)	Corresponding estimated work function, ϕ (eV)
Before max. temp.	750	4.03	3.95
Max. temp.	1085	4.61	4.52
After max. temp.	750	4.69	4.61

Considering that the dominant peak at and after the maximum temperature corresponds to a work function very similar to that of graphite 4.6 eV [30], we believe that the high temperature caused the termination layer to desorb such that the majority of emitted electrons derive from regions on the surface that contain π -bonded carbon atoms as a result of the loss of the hydrogen surface termination. The nanocrystalline diamond film also has a high fraction of exposed grain boundaries where π -bonded carbon is known to exist [31,32].

The partial pressures in the vacuum chamber during the heating cycle confirm the hypothesis that the surface termination is unstable at these temperatures. Fig. 5 shows a mass spectrum based on partial pressures of molecules in the vacuum chamber measured simultaneously with the TEEDs. A mass-to-charge ratio of 18 (corresponding to H_2O) represents the largest partial pressure for all conditions, and its presence is reduced significantly by the heating cycle. The inset highlights three particular charge-to-mass ratios, 1 (H), 2 (H_2) and 16 (CH_4) that would likely be present upon desorption of atomic H or CH_3 groups. According to the inset in Fig. 5, H_2 occupied a slightly greater percentage of the vacuum chamber gas after the heating cycle than it did before. These results are contrary to the general trend of diminishing partial pressures witnessed in the other measured species. This response may indicate that H_2 has been supplied to the vacuum chamber from the hydrogen-terminated film through a desorption process, but the measurement could also be influenced by the decomposition of water into H_2 .

Recently, Köck et al. [9] published results of field emission from surface-treated N-doped diamond films at elevated temperatures. They observed a decrease in current at 725°C and attributed the decrease to the instability of the hydrogen surface layer at temperatures above 725°C. Furthermore, Hamza et al. [33] observed that hydrogen on diamond desorbs at temperatures between 800 and 1000°C (~1100–1300K) in UHV and concluded that both surface-adsorbed and near-surface adsorbed hydrogen is released. The TEEDs measured in this study support the hypothesis offered by Köck et al. Assuming that the low-energy peak represents emission from a hydrogen-terminated region, one can conclude that the hydrogen layer has become unstable, and that electrons begin to experience a generally higher work function at or slightly above 750°C.

5.3. Nanocrystalline diamond with nitrophenyl adlayer (NND)

Similar to the HND film, the nitrophenyl adlayer was unstable above 750°C, and the maximum thermionic electron

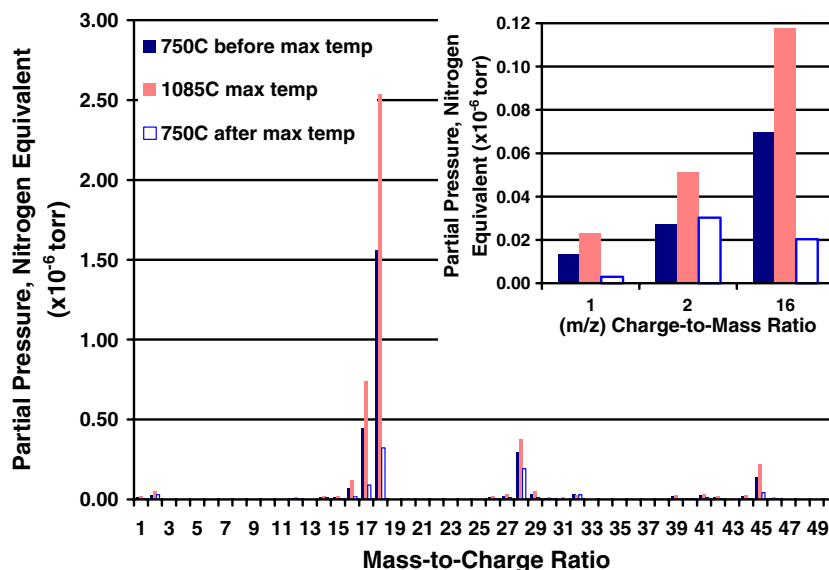


Fig. 5. Mass spectra from hydrogen-terminated nanocrystalline diamond at 750, 1085 and again at 750 °C. The inset displays the partial pressure of three particular mass-to-charge ratios (1 and 2, and 16) corresponding to H, H₂, and CH₄, respectively. These species may form during desorption of the hydrogen termination layer.

intensity for this sample shifted to higher energy after heating to the maximum temperature, as illustrated in Fig. 6. The initial TEED at 750 °C exhibits a similar peak followed by a higher-energy shoulder, which becomes the dominant peak at the maximum temperature (1089 °C) and at 750 °C after the maximum temperature. Comparing the data in Table 1 with that in Table 2 below, it is clear that at the maximum temperature and above, the energy distributions are dominated by emission from a region with an effective work function in the range 4.53 to 4.61 eV. Also, before the maximum temperature, the NND film exhibited the lowest recorded effective work function, 3.88 eV.

RGA data were recorded simultaneously with the TEEDs during tests on the NND sample. The inset in Fig. 7 highlights the partial pressures of the benzene groups ($m/z=77, 78$), NO, and the admolecule ($m/z=123$), which are likely products of a nitrophenyl desorption process. In this case, the species' pre-

sence in the vacuum chamber diminished throughout the heating cycle. Even when the temperature increased to a maximum (1089 °C), the partial pressure did not exceed its initial value at 750 °C. One explanation for this behavior is that the partial pressure of benzene groups had peaked due to desorption from the surface before the TEED at maximum temperature and corresponding residual gas partial pressures were measured (the time required to increase temperature from 750 °C to the maximum temperature was approximately 30 min). Then, when the measurements were carried out at maximum temperature, the partial pressure of the benzene groups had decreased because the supply from the sample emitter's surface had already been exhausted.

5.4. Nanocrystalline diamond with re-generated hydrogen termination

After recording the results for the HND sample described in Section 5.2, hydrogen termination was regenerated in a PECVD system, and the sample's thermionic performance was re-assessed. The hydrogen plasma treatment was performed at 800 W, 200 sccm H₂, 30 Torr and approximately 780 °C for 10 min. Subsequently, the re-generated nanocrystalline diamond (R-HND) film was slowly cooled in the presence of atomic

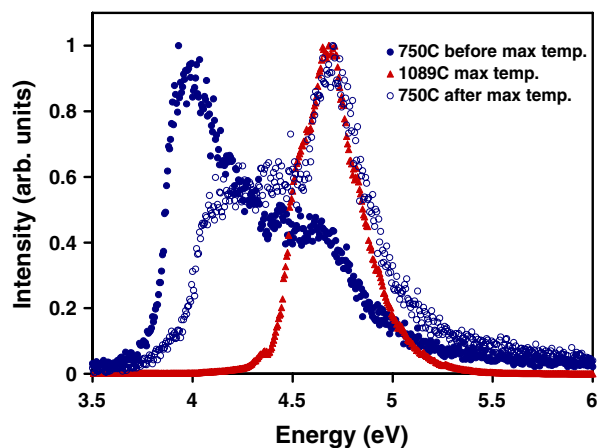


Fig. 6. Sequential TEEDs from nanocrystalline diamond film with nitrophenyl termination measured at 750, 1089 and 750 °C. The shift in the energy at maximum intensity before and after the maximum temperature indicates that the relative area of higher work function has increased in size.

Table 2
Resolution, energy of peak intensity and effective work function of TEEDs from the NND sample

TEED	Temperature (°C)	Energy at max. intensity (eV)	Corresponding estimated work function, ϕ (eV)
Before max. temp.	750	3.96	3.88
Max. temp.	1089	4.66	4.57
After max. temp.	750	4.63	4.55

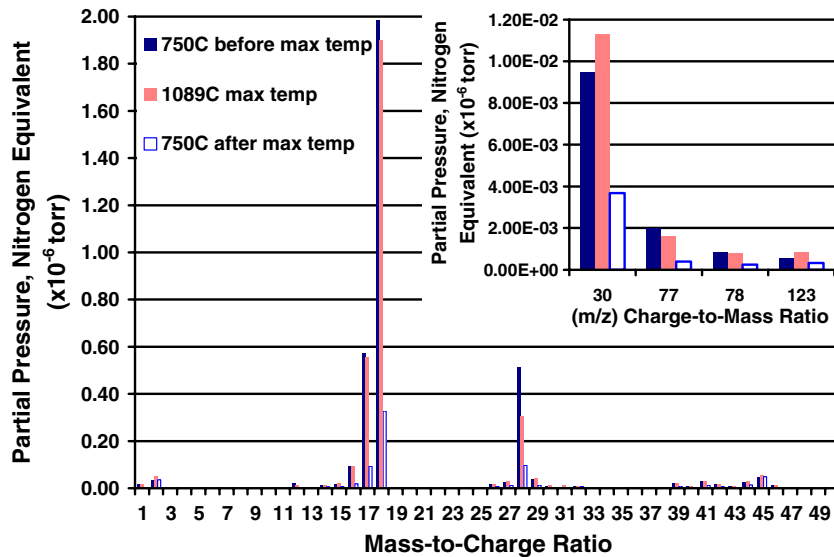


Fig. 7. Mass spectra from nanocrystalline diamond with a nitrophenyl adlayer at 750, 1089 and 750°C. The inset displays the partial pressure of four particular mass-to-charge ratios (30 and 77, 78 and 123) that correspond to NO, benzene (77 and 78), and the molecular ion of the admolecule, respectively. These species are likely present during desorption of the nitrophenyl termination layer.

hydrogen as discussed *vide supra*. After restoring the surface termination, TEEDs were measured during another heating cycle up to a maximum temperature of 940°C.

Similarly to the previous samples, heating the R-HND appeared to cause desorption of the surface termination layer. Fig. 8 contains TEEDs measured at 700, 750 and 850°C. For temperatures at and below 750°C, thermionic emission was stable, with repeatable TEEDs. However, at 850°C, the location of peak intensity increased by approximately 0.9 to 4.8 eV. The effective work function of the R-HND sample below 750°C was approximately 3.9 eV as determined by curve-fitting Eq. (4) assuming a single work function. With 95% confidence, the root mean square errors in the curve-fits for all data in Fig. 8 were less than 0.026, and the *R*-square values were greater than 0.965.

Fig. 9 re-plots the 750°C R-HND data and the corresponding curve fit and also illustrates that the shift in work function with increasing temperature is an irreversible process. The curve-fit for

the TEED at 750°C is representative of the excellent agreement between theoretical and experimental distributions. In this particular case, the root mean square error was 0.004, and the *R*-square value was 0.999. The TEED at 900°C in Fig. 9 is consistent with that at 850°C in Fig. 8. After dwelling at a maximum temperature of 940°C, the sample temperature was decreased with TEEDs recorded at 800, 750, and 700°C. Once the distribution had shifted to higher energy as shown in Fig. 8, the distributions were very consistent at all temperatures and exhibited work functions between 4.81 and 4.85 eV. Each of these distributions was analyzed with the curve-fitting procedure described above, and Table 3 lists the most relevant parameters of each. These results for the R-HND sample indicate a permanent work function increase of approximately 0.9 eV.

Comparison of the TEED shapes for the three tested samples (HND, NND, R-HND corresponding to Figs. 4, 6, and 9),

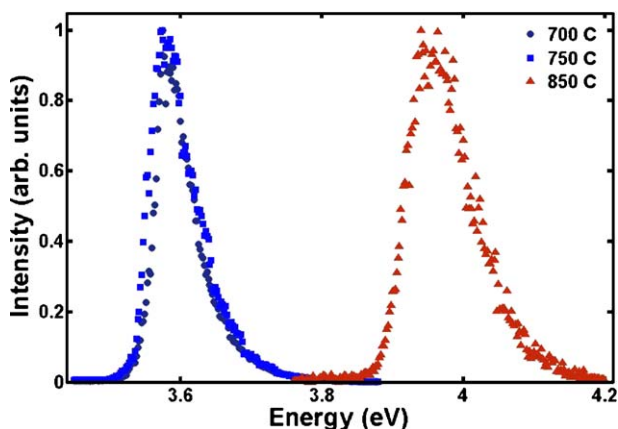


Fig. 8. TEEDs from R-HND at 700, 750 and 850°C. Distributions were consistent below 750°C, and again after 850°C. The shift in energy of the distribution is attributed to desorption of hydrogen from the surface.

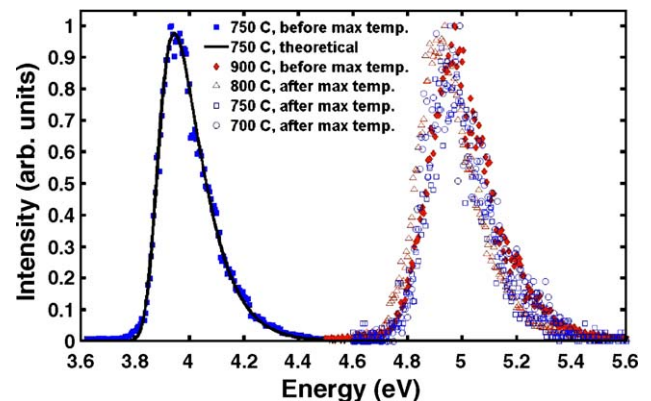


Fig. 9. The shift to higher energies was permanent, as demonstrated by the constant distribution with varying temperature. The TEEDs at 800, 750, and 700°C were measured after the sample had been heated to a maximum temperature of 940°C. A representative curve fit at 750°C is included. Curve fits were used to estimate the work function of the R-HND sample.

Table 3
Summary of curve-fitting results for the regenerated HND (R-HND) before and after maximum temperature

Temperature (°C)	Estimated work function (eV)	Analyzer resolution, σ (eV)	R^2
750, before max temp	3.86	0.030	0.999
900, before max temp	4.85	0.067	0.997
800, after max temp	4.81	0.052	0.998
750, after max temp	4.85	0.052	0.989
700, after max temp	4.81	0.030	0.964

Analyzer resolution σ is defined in Eq. (3). R^2 represents the proportion of variation explained by the model [35] and varies between 0 and 1, with a value of unity representing an ideal model.

respectively) suggests that, for the former two samples, a mixture of regions of different work functions exists across the surfaces, as indicated by the shoulders in the distributions. Heterogeneities in the electrical and electrochemical properties across the surface of polycrystalline, boron-doped diamond films are well known and have recently been investigated by conducting probe atomic force microscopy (CP-AFM) and scanning electrochemical microscopy (SECM) [34]. However, the distributions from the re-generated hydrogen-terminated surface conform well to a single-work-function model.

This result suggests that a change occurred in the chemical and/or electronic properties of the surface after rehydrogenation. One possible explanation is the loss of much of the π -bonded grain boundary carbon due to hydrogen chemisorption. The initial nanocrystalline diamond film has at least two general sites for emission: the hydrogen terminated sp^3 -bonded carbon of the diamond grains and the sp^2 -bonded carbon in the grain boundaries. Extended phases of sp^2 -bonded carbon do not exist in the grain boundaries. The latter sites are expected to have a higher work function than the former. After the hydrogen plasma treatment, it is possible that much of the sp^2 -bonded grain boundary carbon has been transformed to a sp^3 bonding configuration. The possibility of some etching exists, although the morphology of the films is unaltered after plasma treatment, but the primary modification is hydrogen chemisorption, leading to a surface with a more homogeneous work function. Another possible explanation is that the electrical conductivity across the surface is more uniform after rehydrogenation. Recent CP-AFM measurements support this latter supposition as it was observed that the electrical conductivity is more uniform over a boron-doped nanocrystalline diamond surface after hydrogen plasma treatment.

6. Conclusions

The present work indicates that hydrogen and nitrophenyl termination layers on the surface of boron-doped nanocrystalline diamond become unstable at temperatures near 750°C. Comparisons of TEEDs at approximately 750°C before and after heating to a higher temperature reveal a large, upward shift in effective work function. Partial pressure measurements for the hydrogen-terminated surface indicate an increase in molecular hydrogen after heating to the maximum temperature, but similar experiments on species associated with the nitrophenyl did not

exhibit such an increase. In all cases, the increase in work function occurred near 750°C, but the shapes of the distributions differed in that those from the original hydrogen- and nitrophenyl-terminated samples showed shoulders that were indicative of multiple work functions while the re-generated hydrogen-terminated surface produced distributions corresponding to a single work function. Consistent with this are (i) the variations we have recently detected in the apparent work function across the surface of boron-doped diamond films using scanning Kelvin-probe force microscopy and (ii) the variations in electrical conductivity across the surface of a boron-doped diamond film as detected by conductivity-probe atomic force microscopy [34]. The variability in the work function deserves further examination, as uniformity of emission is an important consideration in the application of thermionic emission materials in practical devices.

Acknowledgements

The authors gratefully acknowledge financial support for this work through the National Science Foundation (NIRT 0210336), and Matt Maschmann's assistance in producing the SEM images.

References

- [1] G.P. Smestad, *Sol. Energy Mater. Sol. Cells* 82 (2004) 227.
- [2] G. Miskolcay, D.P. Lieb, *Proc. Intersoc. Energy Convers. Eng. Conf., Inst. Electric. Electron. Eng., Reno, Nevada, , 1990, p. 222.*
- [3] H. Oman, *IEEE Aerosp. Electron. Syst. Mag.* 18 (2003) 28.
- [4] V.I. Yarygin, Ye.A. Meleta, S.M. Tulin, V.V. Klepikov, V.A. Ruzhnikov, L.R. Wolff, *Proc. Intersoc. Energy Convers. Eng. Conf., Inst. Electric. Electron. Eng., Monterey, California, , 1994, p. 1061.*
- [5] T.H. Van Hagan, J.N. Smith Jr., *Proc. Intersoc. Energy Convers. Eng. Conf., Inst. Electric. Electron. Eng., Washington, D.C., 1996, p. 629.*
- [6] S.W. Angrist, *Direct Energy Conversion*, Allyn and Bacon, Inc., Boston, 1965.
- [7] K.L. Thayer, M.L. Ramalingam, T.R. Lamp, *Proc. Int. Mech. Eng. Conf. Expo., Am. Soc. Mech. Eng., Chicago, IL., 1994, p. 1.*
- [8] T.S. Fisher, *Appl. Phys. Lett.* 79 (2001) 3699.
- [9] T.S. Fisher, D.G. Walker, *J. Heat Transfer* 124 (2002) 954.
- [10] V.S. Robinson, T.S. Fisher, J.A. Michel, C.M. Lukehart, *Appl. Phys. Lett.* 87 (2005) 061501.
- [11] F.A.M. Köck, J.M. Garguilo, B. Brown, R.J. Nemanich, *Diamond Relat. Mater.* 11 (2002) 774.
- [12] J.B. Cui, J. Ristein, L. Ley, *Diamond Relat. Mater.* 9 (2000) 1143.
- [13] L. Diederich, O.M. Küttel, P. Aebi, L. Sclapbach, *Diamond Relat. Mater.* 8 (1999) 743.
- [14] T.-C. Kuo, R.L. McCreery, G.M. Swain, *Electrochem. Solid-State Lett.* 6 (1999) 288.
- [15] J. Pinson, F. Podvorica, *Chem. Soc. Rev.* 34 (2005) 429.
- [16] J.W. Gadzuk, E.W. Plummer, *Rev. Mod. Phys.* 45 (1973) 487.
- [17] R.D. Young, *Phys. Rev.* 113 (1959) 110.
- [18] A.C. Marshall, *Surf. Sci.* 517 (2002) 186.
- [19] R.D. Young, C.E. Kuyatt, *Rev. Sci. Instrum.* 39 (1968) 1477.
- [20] R. Reifenberger, H.A. Goldberg, M.J.G. Lee, *Surf. Sci.* 83 (1978) 599.
- [21] I. Brodie, P.R. Sewoebel, *Proc. IEEE* 87 (1994) 1006.
- [22] G. Popovici, M.A. Prelas, *Phys. Status Solidi, A* 132 (1992) 233.
- [23] M. Delamar, R. Hitmi, J. Pinson, et al., *J. Am. Chem. Soc.* 114 (1992) 5883.
- [24] A.O. Solak, L.R. Eichorst, W.J. Clark, R.L. McCreery, *Anal. Chem.* 75 (2003) 296.
- [25] J. Wang, M.A. Firestone, O. Auciello, J. Carlisle, *Langmuir* 20 (2004) 11450.

- [26] M.A. Brown, L. Neelands, H. Farnsworth, *J. Appl. Phys.* 21 (1950) 1.
- [27] M. Nichols, *Phys. Rev.* 57 (1940) 297.
- [28] G. Smith, *Phys. Rev.* 94 (1954) 295.
- [29] R.D. Young, *Phys. Rev.* 113 (1959) 110.
- [30] R.C. West, *CRC Handbook of Chemistry and Physics*, CRC Press, 1976.
- [31] D.M. Gruen, *Annu. Rev. Mater. Sci.* 29 (1999) 211.
- [32] J. Birrell, J.E. Gerbi, O. Auciello, J.M. Gibson, D.M. Gruen, J.A. Carlisle, *J. Appl. Phys.* 93 (2003) 5606.
- [33] A.V. Hamza, G.D. Kubiak, R.H. Stulen, *Surf. Sci.* 237 (1990) 35.
- [34] K.B. Holt, A.J. Bard, Y. Show, G.M. Swain, *J. Phys. Chem., B* 108 (2004) 15117.
- [35] N.R. Draper, H. Smith, *Applied Regression Analysis*, Third Edition, John Wiley and Sons, Inc., New York NY, 1998.